Energy Harvesting Wireless Sensor Network Edge Device Simulation Tool

Cian O'Shea, Ross O'Halloran, Peter Haigh, Mike Hayes
Tyndall National Institute
Cork, Ireland
Email: cian.oshea@tyndall.ie

***Abstract* - Wireless Sensor Networks (WSN) are becoming widely adopted in many industries including health care, building energy management and conditional monitoring. As the scale of low-power sensor network deployments increases, the cost and complexity of battery replacement and disposal have become more significant and in time may become a barrier to adoption. Harvesting ambient energies provides a pathway to reducing dependence on batteries and for many application scenarios, may lead to autonomously powered sensors. This work describes a simulation tool that enables the user to predict the battery life of a wireless sensor that utilizes energy harvesting to supplement the battery power. To create this simulator, all aspects of a typical WSN edge device (node) were modelled including sensors, transceiver and microcontroller as well as the energy source components (batteries, solar (PV) cells, Thermoelectric Generators (TEG), supercapacitors and DC/DC converters). The tool allows the user to plug and play different pre-characterized devices as well as add user defined devices. The goal of this simulation tool is to provide a WSN installer with a methodology to deploy systems with optimum battery lifetime by scaling battery and energy harvesting component sizes appropriately for a given scenario. It also allows a component designer to examine trade-offs in system level performance versus device specifications for optimum battery lifetime.**

Keywords – Wireless Sensor Network; Low-power sensor network; Internet of Things (IoT); Energy Harvester; simulation tool

I. INTRODUCTION

With the ever-increasing push to have a more energy efficient environment, the retrofit of IoT edge devices, such as wireless sensors in, on or near equipment and its operating environment is becoming more prevalent to help gather data to achieve this goal. Commercial and residential buildings are now expected to meet better and higher standards of energy efficiency, with the Irish government mandating that all newly constructed buildings require at least 20% of the energy needs be sourced through renewable energy [1].

The deployment of IoT devices is growing at an exponential rate. By 2025 there will be an estimated 75 billion IoT devices worldwide [2] most of which, will be wireless. One of the biggest challenges that IoT devices face is battery life. With so many devices globally, this is a serious issue. According to the United States Environmental Protection Agency, roughly 90% of batteries are recycled [3]. By 2025, that still leaves 7.5 billion batteries filling landfills and polluting the earth. Combine this with the environmental cost of mining the material used and the monetary cost of producing so many batteries, technologies such as energy harvesting that enable battery life to be extended are highly desirable. The simulation tool presented in this paper will allow a user to select from a range of different components to extend the battery life of their IoT end nodes by installing more cost effective, lower maintenance overhead and energy efficient device.

Energy harvesting is the act of collecting ambient energy from the environment and either converting it into device-ready electrical energy or storing it. The environment has readily available ambient sources of energy. Energy harvesting can be very beneficial for WSN nodes. This software tool will allow people to see the usefulness of energy harvesting and how real-world applications can be completely powered or have their battery life extended with the use of an energy harvesting system. This tool will encourage the use of ambient energies, particularly in applications that would greatly benefit from averting or prolonging the need for battery replacement, for example in hard to reach areas such as civil engineering structures and medical implants.

In Section 2 this paper will present the simulation tool and discuss its operation. Section 3 will then describe WSN and the different components involved. Section 4 will present the user interface of the simulation tool and illustrate what a typical user would see. Sections 5 to 10 will then describe each component and its characterization methods. The results in Section 11 will show a comparison between a real-world test and software simulation, showing the accuracy of the tool. The final Section will present the conclusions drawn and propose several possible directions for future work.

II. SOFTWARE TOOL

Energy harvesting is a common method used to extend the battery lifetime in WSN devices. The software application described in this paper has two purposes:

1. It can be used by component designers to trade off system performance against component performance in an end node.
2. It can also be used by a system integrator as a validation tool during the development process of the WSN system. It will allow a user to determine if the ambient energy available to the

 ISBN: 978-1-61208-819-8

device is enough to sustain it or prolong the battery lifetime for a desired period.

One of the main goals of this software tool was to have the ability to predict lifetime for any given node. This allows a user to import any type of component to the software using the predetermined characterisation structure and predict the lifetime of the WSN node using a given combination of power generation, storage and consumption components.

III. WIRELESS SENSOR NETWORK

A WSN consists of a gateway, which receives all of the data from the connected nodes in the network and then transmits that data to the cloud, as shown in Figure 1.

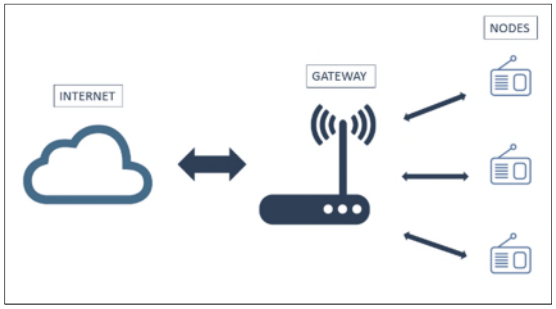

Figure 1. Example of a WSN.

The focus of this simulation tool is predicting the lifetime of the nodes in the network by importing characterized components and flowing that data through a set of equations to accurately predict the lifetime of the device. A typical node in a WSN that utilizes Energy Harvesting (EH-WSN) methods consists of the following parts; an energy harvester, a power-management IC, which includes a Maximum Power Point Tracker (MPPT), an energy storage device, a DC-DC converter and finally a sensor (or cluster of sensors).

Figure 2 represents a block diagram of an EH-WSN.

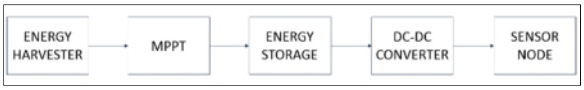

Figure 2. EH-WSN block diagram.

The energy harvester transducers that are available with the simulation tool developed are PV cells and TEGs. With the ambient energy available (e.g., light, heat) usually being quite limited and sporadic, any change in environmental conditions throughout the harvesting period can have a significant effect on the amount of energy that the EH (energy harvesting) transducers can provide. For this reason, an MPPT circuit is required to maximise the power output from the transducer to the load. Because of the uncertainty in available power from energy harvesting, an energy storage device is required to maintain constant power to the sensor node. An energy storage device can provide power to the load when the ambient energy is unavailable, but it can also, store excess energy when the transducers are harvesting more energy than the load requires. Supercapacitors, also known as ultracapacitors or double-layer capacitors, are commonly used in EH-WSNs as they have a higher power density than batteries and can operate without the need for additional charging circuitry. They also have a long operational lifetime, with charging and discharging of the device having little to no effect on it [4]. However, as the voltage in the device is varying, a DC-DC converter is required to maintain a stable voltage on the sensor node, which typically contains a receiver, transmitter and a microprocessor. Primary batteries are also used for energy storage, with the choice being dependent on application powering requirements. These additional batteries may also require a DC-DC converter.

IV. GUI

When the application launches, the user can vary any of the parameters in a WSN by selecting the button that corresponds to that section. These buttons can be seen in Figure 3.

Figure 3. GUI buttons.

In Figure 4, the user can input the operating voltage and the average current consumption of the device which then gets sent to the main simulation file and awaits further data.

 ISBN: 978-1-61208-819-8

Figure 4. Sensor Node menu.

The two types of EH devices available in this simulation tool are PV cells and TEGs whose parameters can be modified in Figure 5. Other types can be easily added. The user can select which type and then either select from pre-characterised components in the tool or add a new component to the simulation. This allows users to import their own components to test their viability in a WSN system. The size of the components and ambient conditions must also be selected.

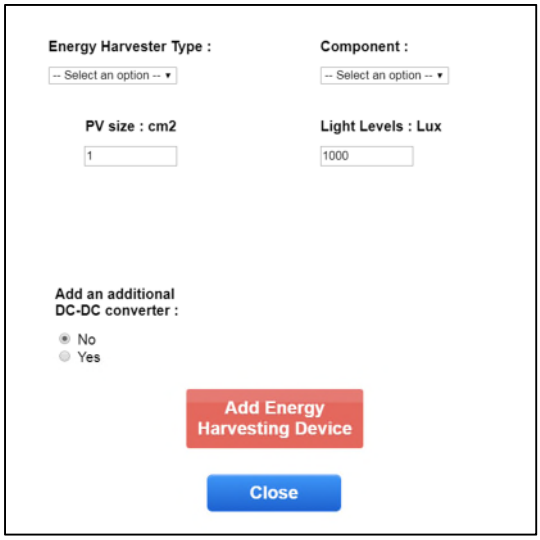

Figure 5. EH menu.

Similar to the EH section, Figure 6 shows that the user can enter the parameters of the supercapacitor or import a new component. The minimum and turn on voltage of the supercapacitor can also be selected. This notifies the simulation that once the supercapacitor reaches the minimum voltage, it must be allowed time to recharge back to the turn on voltage and disconnected from the load. This allows the system to alternate between powering the sensor node using EH methods and using battery power.

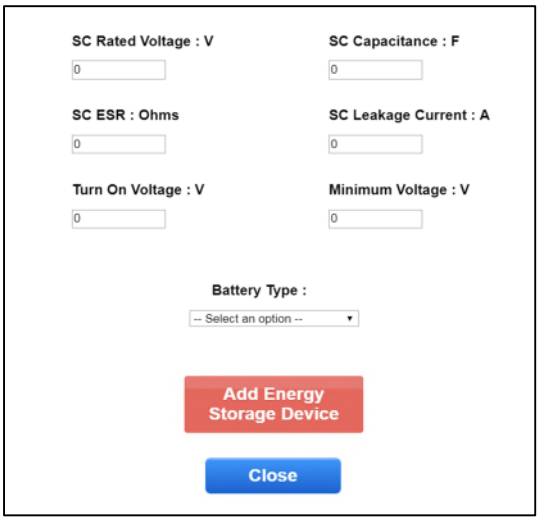

Figure 6. Supercapacitor menu.

Figure 7 shows a selection window for a DC-DC converter. As was mentioned previously, the system requires a DC-DC converter to maintain a constant voltage to the sensor node. Depending on the minimum and maximum input voltages of the device, it may influence the operating limits of the supercapacitor. The rated voltage of the supercapacitor should be checked to see if it is compatible with the DC-DC converter.

Figure 7. DC-DC converter menu.

Once all of the parameters are selected, a simulation window is presented to the user. Figure 8 shows a complete simulation, illustrating the effects of the

minimum and turn-on voltages. Figure 9 compares the lifetime of the device when powered solely by battery (shown in red) and a battery-EH hybrid system (shown in blue).

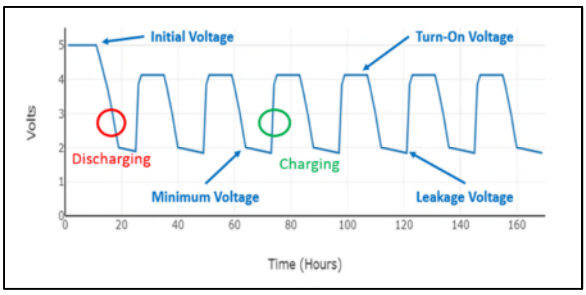

Figure 8. Supercapacitor voltage over time.

As the simulation is running, the graph presented in Figure 8 is shown. This allows the user to see when the supercapacitor reaches its minimum or maximum voltage and can alter the components to achieve the optimum power solution to the device, whether the supercapacitor is receiving too much energy or too little. It also allows the user to check whether or not the supercapacitor is sized correctly or the DC-DC converter suitable for the system. Figure 8 also shows that when the supercapacitor reaches the minimum voltage and there is no ambient energy available, the voltage continues to drop due to leakage current before the charging cycle starts again.

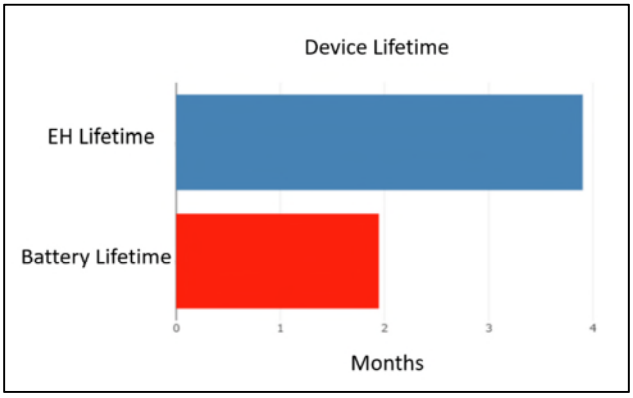

Figure 9. Battery WSN vs. EH-WSN.

Altering the input parameters to the system allows the user to determine the optimised component setup to power the device.

Once the simulation has begun, bars shown in Figures 10-12 will present the ongoing conditions in the system over time. When there is no ambient energy available to the system (e.g., lights switched off), the yellow bar is depleted signalling that the supercapacitor is no longer receiving energy. This can be seen as the simulation is displayed. Figure 11 is a representation of the green circle shown in Figure 8. The device is receiving ambient energy and charging. Figure 12 is a representation of the red circle. There is no ambient energy available and the supercapacitor is roughly 50% charged.

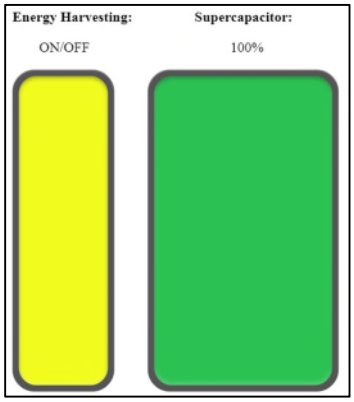

Figure 10. Simulation dynamic conditions.

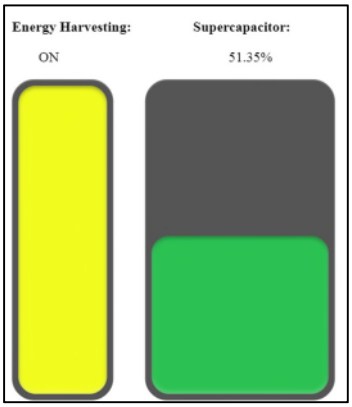

Figure 11. Simulation dynamic conditions.

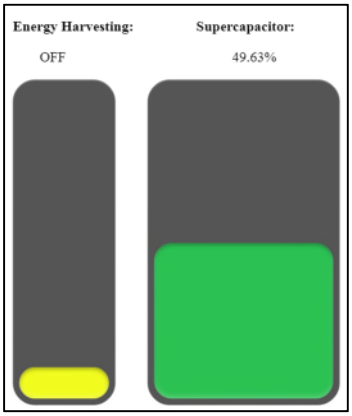

Figure 12. Simulation dynamic conditions.

As the WSN switches between the use of EH and the use of a battery, that too is shown to the user with the EH bar toggling on or off and the supercapacitor bar increasing or

decreasing. If the supercapacitor reaches the minimum voltage, it requires time to recharge, which switches the device to receive power from the battery. Figures 13 and 14 represent when the device is receiving ambient energy or not respectively.

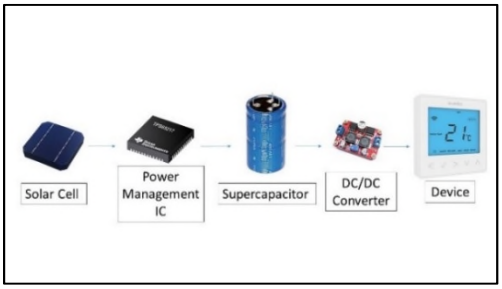

Figure 13. Using EH indicator.

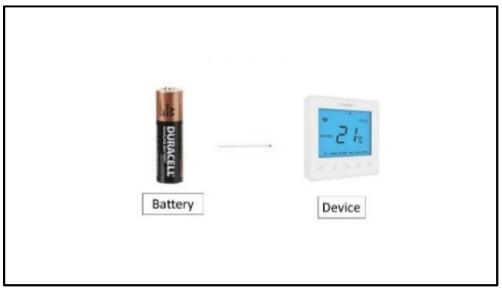

Figure 14. Using battery indicator.

What makes this different from other WSN simulators, is its ability to import new components and allow users to use their own or test components they are thinking of acquiring. The characterisation templates are included with the software and that data can mostly be found in the datasheets of the components or easily derived from some bench testing.

V. ENERGY HARVESTER

PV cells can be characterised by using what is termed “I-V & P-V curves”. They represent the relationship between the electric current/power through the cell with the corresponding voltage for different light intensity levels. These curves can then be used to find the maximum power point.

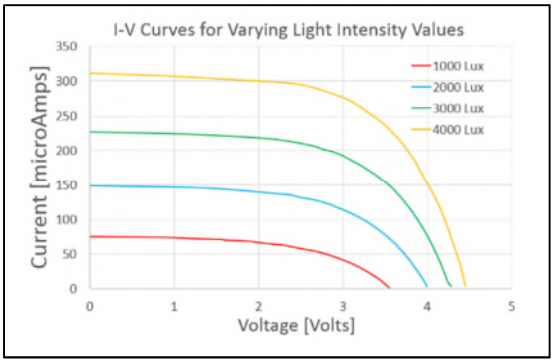

(a)

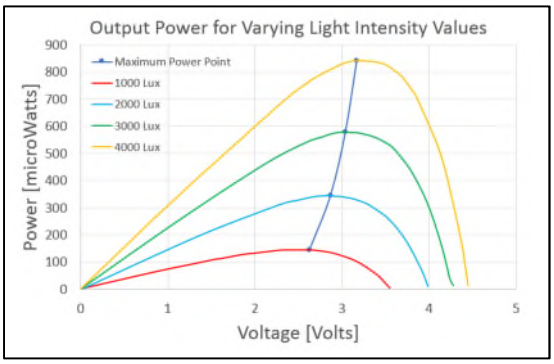

(b)

Figure 15. (a) I-V curves for varying light intensity levels. (b) Output power for varying light intensity levels.

Figure 15(a) shows how different lux levels can affect the current generated by the PV cell whilst Figure 15(b) presents the maximum output power of the PV cell for each lux value. An MPPT circuit can be used to help the PV cell operate at its maximum power point.

Thermoelectric generators work by taking advantage of the Seebeck effect, which directly converts temperature difference into electricity. When heat is applied to one of the two conductors in the TEG, the temperature of electrons close to the surface begin to rise and flow towards the cooler surface creating current flow. When a temperature difference exists on the P-N junctions, a potential voltage difference between the hot and cold surfaces occurs [5].

Similarly to a PV cell, a TEG is also characterised using “I-V curves” and “P-V curves” and impedance matching circuits can be used to obtain a maximum power point, which can be seen in Figures 16 (a) & (b).

 ISBN: 978-1-61208-819-8

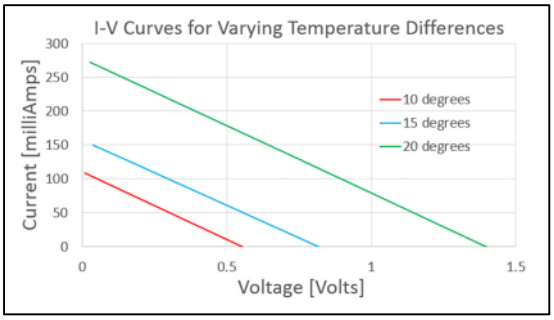

(a)

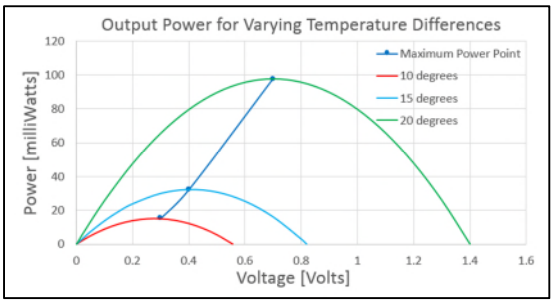

(b)

Figure 16. (a) I-V curves for varying temperature differences. (b) Output power for varying temperature differences.

VI. MAXIMUM POWER POINT TRACKER FOR PV

The MPPT used in this simulation tool for PV is called Fractional Open-Circuit Voltage (FOCV). This method is based on the fact that the voltage of the PV cell at the maximum power point (V_{MPP}) is approximately linearly proportional to the open-circuit voltage (V_{OC}) and short-circuit current (I_{SC}) based on the following equations:

$$V_{MPP} \approx K_1 * V_{OC} \quad (1)$$

$$I_{MPP} \approx K_2 * I_{SC} \quad (2)$$

where the value for K_1 ranges from 0.7-0.9 and K_2 ranges from 0.78-0.92 depending on the overall characteristics of the solar cell.

A flowchart of the FOCV algorithm is represented in Figure 17.

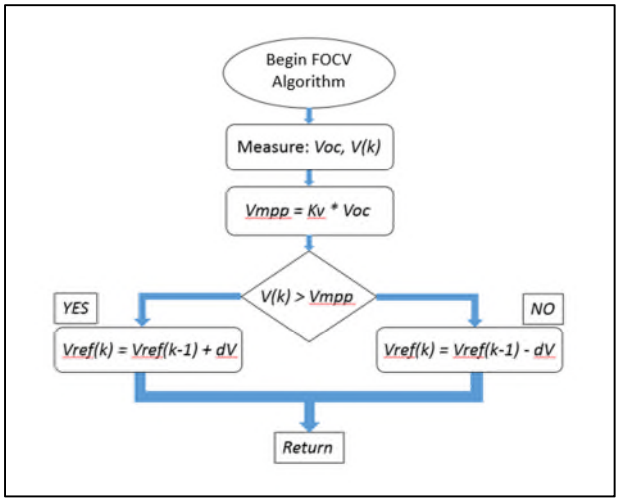

Figure 17. Fractional Open-Circuit Voltage algorithm.

From [6]-[8], it was concluded that the FOCV method was the best fit for ultra-low-power sensor networks (sub mW power levels) with an accuracy rating of 96%, which is the value used in this simulation tool.

$$MPP_{CHARACTERIZED} * 0.96 \approx P_{EH} \quad (3)$$

Where $MPP_{CHARACTERIZED}$ is maximum characterized power of the EH after it has gone through a MPPT circuit and P_{EH} is the EH power used in the simulation.

VII. ENERGY STORAGE

For optimum energy efficiency, an energy storage device is required to store any excess energy generated by the energy harvester transducers. This stored power can then be used to power the sensor node when ambient energies are no longer available in order to prolong the lifetime of the battery. A battery is used when ambient energy is not available, and the power stored in the supercapacitor is depleted. In this simulation tool, a supercapacitor is modelled in unison with a single-use battery. Taking values, such as capacitance, rated voltage, leakage current and Equivalent Series Resistance (ESR), the energy in the supercapacitor can be simulated as it charges and discharges. ESR is a non-ideal characteristic of a supercapacitor and can cause problems when dealing with I^2R losses and transients. The bigger the load transient, the larger the voltage drop due to ESR. The equations governing the supercapacitor in this simulation are shown in the results section.

VIII. DC-DC CONVERTER

When powering systems from ambient energy the designer should ensure that as much power as possible that is generated by the transducer is delivered to the load. Techniques to reduce power losses need to be employed. In this case the supercapacitor voltage will vary during charge and discharge, therefore a DC-DC converter is

 ISBN: 978-1-61208-819-8

required to ensure the load is supplied with the appropriate steady voltage level at maximum efficiency. The output power to the load is based entirely on the specified output voltage of the converter and the current consumption of the sensor node. The power required at the input is dependent on the voltage at the input. As the voltage at the input varies, so too does the efficiency of the converter. This also varies the power required from the supercapacitor to maintain constant power to the output. In this software tool, the user selects an average efficiency rating of the converter and then integrates top and bottom thresholds. At these points, when the voltage reaches those levels, the efficiency changes. This can be further explained in table 1.

TABLE I. DC-DC CONVERTER EFFICIENCY FOR DIFFERENT INPUT VOLTAGES

Input Voltage Range (V)	Efficiency (%)
5 – 4.2	84.5
4.2 – 3.6	86
< 3.6	90

$$\eta \approx \frac{Voltage_{OUT} * Current_{OUT}}{Voltage_{IN} * Current_{IN}} \quad (4)$$

where $Voltage_{IN}$ and $Current_{IN}$ are the input voltage and current to the DC-DC converter respectively (i.e., the WSN node).

Furthermore:

$$Supercapacitor\ Power \approx \frac{Node\ Power}{\eta} \quad (5)$$

Where "Supercapacitor Power" is power required by the supercapacitor to maintain constant power to the node. The efficiency value is also determined by the operating supercapacitor voltage. As the voltage in the supercapacitor changes with time, the efficiency at which the DC-DC converter converts the input power of the supercapacitor to the required power levels of the sensor node changes.

IX. SENSOR NODE

The sensors in these nodes typically have different operating modes, for which their period of operation is defined by their different duty cycles. The average power then depends on the power consumed in each operation mode as well as the time employed for each mode (i.e., the 'duty cycle'). The simulation tool handles this by taking in the average current consumption level for a specific duty cycle and using the operating voltage to determine the power required.

$$WSN\ Power = Voltage * Average\ Current \quad (6)$$

X. SIMULATION

To ensure that simulation results are accurate, the individual components need to be characterized in a uniform manner under operating conditions that reflect real life. The wide range of component types makes this challenging. However, by doing this, an extensive array of components can be catalogued and stored in the software for comparison and to assess their viability for different applications.

The simulation tool takes in CSV files containing the required information to model each component. These CSV files have data templates, which can be filled out and logged in the software.

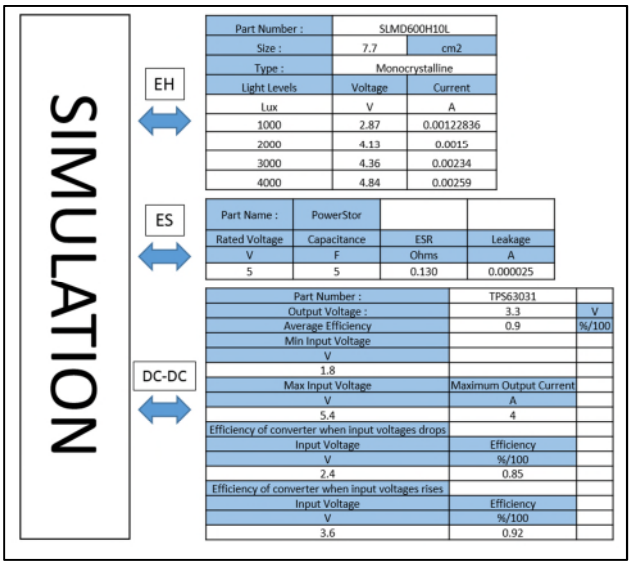

Figure 18. Component characterization templates.

Figure 18 shows the different templates for the energy harvester transducers, the energy storage devices, the DC-DC converters and the sensor nodes.

Other software tools that simulate WSNs are usually manufacturer specific. One of the unique selling features of this simulation tool is that it allows for myriads of combinations and offers the ability to add any type of component to the software.

XI. RESULTS

To test the accuracy of the simulation tool, a circuit was setup to power a LoPy4. The LoPy4 is a low-power radio module that is a typical communication device used in wireless sensors. The module supports, LoRa, Sigfox,

 ISBN: 978-1-61208-819-8

Bluetooth and Wi-Fi. For these experiments it was set up using LoRa.

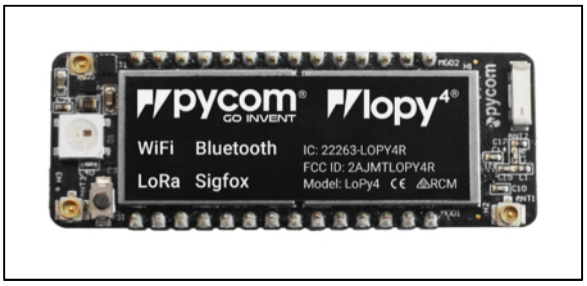

Figure 19. LoPy4 Pycom Device.

During the test, the device shown in Figure 19 was programmed to operate at 90mA. This device was then connected to a supercapacitor, which was then connected to a power supply. Figure 20 shows the circuit schematic of the performed test with the accompanying equations. The goal of this test was to measure the voltage of the supercapacitor as it charged and discharged to compare with a simulated test under the same conditions. The voltage across the supercapacitor was recorded using a Bluno V2.0 board with a ±0.15V error rate, connected to a laptop.

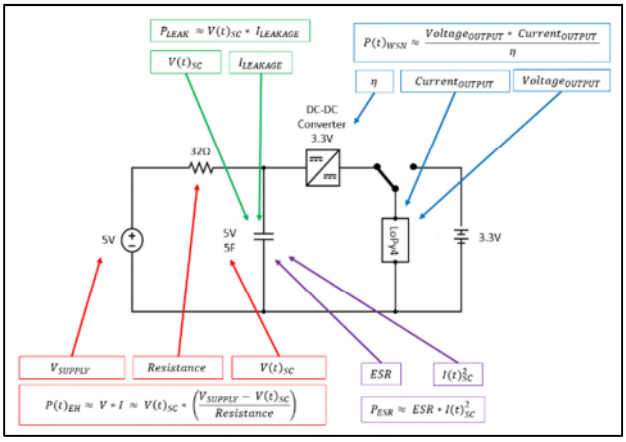

Figure 20. Circuit schematic with equation block diagram.

While the ‘pycom’ device is disconnected and receiving power from the 3V3 supply, the 32Ohm power source mimics an EH transducer. The EH power being fed to the supercapacitor can be approximated using (7). In reality, this power is feeding both the supercapacitor and the DC-DC converter that is operating in ‘no-load’ with the ‘pycom’ disconnected but this is assumed to be very small relative to the current entering the supercapacitor based in quiescent current specifications for the DC-DC converter. Power is a product of current multiplied by voltage. With the voltage constantly varying, so too was the supply current.

$$P(t)_{EH} \approx V(t)_{SC} * I(t)_R \quad (7)$$

$$P(t)_{EH} \approx V(t)_{SC} * \left(\frac{V_{SUPPLY} - V(t)_{SC}}{Resistance}\right) \quad (8)$$

Where $V(t)_{SC}$ is the voltage across the supercapacitor over time and V_{SUPPLY} is the 5V supply voltage.

When the ‘pycom’ is connected to the DC-DC converter, the current and voltage supplied at the input need to be calculated. With losses in the DC-DC converter, more power needs to be supplied than is drawn by the load. The “pycom” device was set at 3.3 volts consuming 90 mA. Using the efficiency equation for DC-DC converter in (4), with the known voltage across the supercapacitor, the current supplied by the supercapacitor can be acquired.

However, as discussed previously the efficiency of the DC-DC converter is dependent on the input voltage. Using the information gathered from the datasheet, the efficiency can be calculated for different operating conditions.

The results in table 1 can then be used to calculate the power supplied to the DC-DC converter and subsequent pycom load (i.e., the WSN node) when not operating off of the 3V3 battery.

$$P(t)_{WSN} \approx \frac{Voltage_{OUTPUT} * Current_{OUTPUT}}{\eta} \quad (9)$$

$$P(t)_{WSN} \approx \frac{3.3 * 0.09}{\eta} \quad (10)$$

TABLE II. WSN NODE POWER REQUIREMENT FOR EACH DC-DC CONVERTER EFICIENCY

Efficiency (%)	$P(t)_{WSN}$ W
84.5	0.3515
86	0.3453
90	0.33

To simplify equations, it is approximated that all of the current for the DC-DC converter comes from the supercapacitor and that the additional current coming from the 32Ohm resistor is very small. This should also offset most of the approximation error for the supercapacitor charge cycle.

The leakage current in the supercapacitor was given in the datasheet as 25µA and equivalent series resistance of 130mΩ. The leakage power can be calculated by multiplying leakage current by the voltage across the supercapacitor.

$$P(t)_{LEAK} \approx V(t)_{SC} * I_{LEAKAGE} \quad (11)$$

Power dissipation due to ESR in the supercapacitor can be calculated by multiplying the ESR value by the square of operating current.

$$P(t)_{ESR} \approx ESR * I(t)_{SC}^2 \quad (12)$$

All of these equations were then fed into (13).

$$E(t)_{SC} \approx E(initial)_{SC} + \int_0^t (P(t)_{EH} - P(t)_{WSN} - P(t)_{LEAK} - P(t)_{ESR})dt \quad (13)$$

where t is the entire period for a given sensing interval. When the supercapacitor has reached its minimum energy availability, the load is disconnected, allowing the supercapacitor to recharge. The "pycom" is switched to receive power from the battery. Using the circuit presented in Figure 20, when the load is disconnected, the DC-DC converter still receives current in the form of quiescent current and the supercapacitor continues to have leakage and ESR losses. This change in current is accounted for in (14), (15) and (16).

$$P(t)_{EH} \approx V(t)_{SC} * \left(\frac{V_{SUPPLY} - V(t)_{SC}}{Resistance} - I_{DC-DC\ Quiescent}\right) \quad (14)$$

$$P(t)_{WSN} \approx 0 \quad (15)$$

$$P(t)_{ESR} \approx ESR * \left(\frac{V_{supply} - V(t)_{SC}}{Resistance} - I_{DC-DC\ Quiescent} - I_{LEAK}\right)^2 \quad (16)$$

$P(t)_{LEAK}$ during this period is still governed by (11).

From there, (17) is used to calculate the voltage in the supercapacitor and then graphed over time to allow the user to continually refine the component parameters in the software.

$$V(t)_{SC} \approx \sqrt{\frac{2*E(t)_{SC}}{C}} \quad (17)$$

Using the minimum voltage specifications from the DC-DC converter of 1.52 volts, the supercapacitor was disconnected from the load and allowed to recharge once it reached that level. It would then switch back to powering the device once it reached 4.6 volts. Using these equations, the results from the simulation were gathered and compared to the real-life test in the following graph.

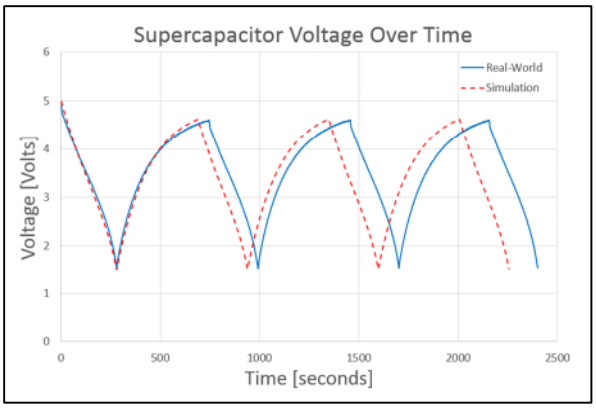

Figure 21. Real-World vs. Simulation comparison.

Figure 21 shows the voltage over time in the supercapacitor for both the real-world and the simulated test as it charges and discharges. Based on these results, the simulation was able to match the supercapacitors discharge profile with 98.9% accuracy while the charge profile predicts with an 89.5% degree of accuracy. In both instances the general shape of the charge/discharge curve looks good except when charging between around 4 and 4.5V, which also creates a net error in the predicted time constant that accumulates with each simulated cycle.

XII. CONCLUSION & FUTURE WORK

In this paper, a simulation tool that predicts the power lifetime of energy-harvested wireless sensor networks is presented. Based on the comparison between a real-world scenario and the simulation data, it can be seen that the software can predict the lifetime of a wireless sensor network with a high degree of accuracy. However, there is a noticeable margin of error in the results. This is likely to be due to a combination of reasons. Firstly, as mentioned, a Bluno V2 board was used to measure the voltage in the "Real-World" test, which had a margin of error of ±0.15V. Also, while the resistor was measured to be exactly 32.77Ohms, the capacitance of the supercapacitor was taken from the datasheet as the rated capacitance. Some simplifying assumptions were used for charging such as taking all the current from the resistor to be entering the supercapacitor when in reality a small percentage will go into the DC-DC converter, acting in quiescent/no load mode. Correspondingly, it is approximated that when the supercapacitor is discharging that all the source current for the DC-DC converter comes from the supercapacitor. However, over a given cycle these approximations should more or less 'balance out' but cause a small net approximation error.

 ISBN: 978-1-61208-819-8

With the implementation of a standardised way of characterising components, this simulation tool provides a much faster method for finding the optimum power setup for a particular application.

For future work, more in-depth analysis of the real-life charging and discharging currents should be undertaken via metrology and closer interaction with the supercapacitor vendor to understand device behaviour particularly in the 4-4.5V charging region. In particular the previously mentioned approximation error assumptions need to be validated and their magnitude assessed. The DC-DC converter will also be in 'no load' rather than quiescent operation so its characteristics in this mode need to be characterised. This should lead to more accurate calculations in future iterations of the model. The way that the software is setup allows for this, as each component has its own separate function, allowing for individual component improvements to the system as a whole. This tool could also be available online where every component added to the system can be available for everyone to use.

ACKNOWLEDGMENT

This work was part of a larger project titled ReCO2ST, (Residential Retrofit assessment platform and demonstrations for near zero energy and CO_2 emissions with optimum cost, health, comfort and environmental quality). This project has received funding from the European Union's "Horizon 2020" research and innovation program under the grant agreement No. 768576.

REFERENCES

[1] SEAI. *Nearly Zero Energy Building Standard* [Online]. Available at: https://www.seai.ie/sustainable-solutions/nearly-zero-energy-buildi-1/ [Accessed 11th June 2019].

[2] Statista. Internet of Things (IoT) connected devices installed base worldwide from 2015 to 2025 (in billions) [Online]. Available at: https://www.statista.com/statistics/471264/iot-number-of-connected-devices-worldwide/ [Accessed 11th June 2019].

[3] EPA. *Sustainable Material Management* [Online]. Available at: https://www.epa.gov/smm [Accessed 5th June 2019].

[4] A. S. Weddell et al. Accurate Supercapacitor Modeling for Energy Harvesting Wireless Sensor Nodes. *Transactions on circuit and systems – II: Express Briefs, 2011*. [Online]. Volume 58, Issue 12, Pages 911-915. Available at: https://ieeexplore.ieee.org/document/6093951 [Accessed 13th May 2019].

[5] C. Hsu et al. An effective Seebeck coefficient obtained by experimental results of a thermoelectric generator module. *Applied Energy* [Online]. Volume 88, Issue 12, Pages 5173-5179, 2011. Available at: https://www.sciencedirect.com/science/article/pii/S0306261911004788#s0010 [Accessed 21st May 2019].

[6] L. Mentally, A. Amghar, H. Sahsah. Comparison between HC, FOCV and TG MPPT algorithms for PV solar systems using buck converter, 2017. [Online]. 2017 International Conference on Wireless Technologies, Embedded and Intelligent Systems (WITS). Available at: https://ieeexplore.ieee.org/document/7934609 [Accessed 6th June 2019].

[7] J. Ahmad. A Fractional Open Circuit Voltage Based Maximum Power Point Tracker for Photovoltaic Arrays, 2010. [Online]. 2010 2nd International Conference on Software Technology and Engineering. Available at: https://ieeexplore.ieee.org/document/5608868 [Accessed 10th June 2019].

[8] D. Baimel, S. Tapuchi, Y. Levron, and J. Belikov, "Improved Fractional Open Circuit Voltage MPPT Methods for PV Systems," Electronics, vol. 8, no. 321, 2019.

 ISBN: 978-1-61208-819-8